

This is the peer reviewed version of the following article:

Geomechanical assessment of the Corvara earthflow through numerical modelling and inverse analysis / Schädler, W.; Borgatti, L.; Corsini, Alessandro; Meier, J.; Ronchetti, Francesco; Schanz, T.. - In: LANDSLIDES. - ISSN 1612-510X. - STAMPA. - 12:3(2015), pp. 495-510. [10.1007/s10346-014-0498-5]

*Terms of use:*

The terms and conditions for the reuse of this version of the manuscript are specified in the publishing policy. For all terms of use and more information see the publisher's website.

06/05/2026 02:41

(Article begins on next page)

## Dear Author

Here are the proofs of your article.

- You can submit your corrections **online**, via **e-mail** or by **fax**.
- For **online** submission please insert your corrections in the online correction form. Always indicate the line number to which the correction refers.
- You can also insert your corrections in the proof PDF and **email** the annotated PDF.
- For **fax** submission, please ensure that your corrections are clearly legible. Use a fine black pen and write the correction in the margin, not too close to the edge of the page.
- Remember to note the **journal title**, **article number**, and **your name** when sending your response via e-mail or fax.
- **Check** the metadata sheet to make sure that the header information, especially author names and the corresponding affiliations are correctly shown.
- **Check** the questions that may have arisen during copy editing and insert your answers/corrections.
- **Check** that the text is complete and that all figures, tables and their legends are included. Also check the accuracy of special characters, equations, and electronic supplementary material if applicable. If necessary refer to the *Edited manuscript*.
- The publication of inaccurate data such as dosages and units can have serious consequences. Please take particular care that all such details are correct.
- Please **do not** make changes that involve only matters of style. We have generally introduced forms that follow the journal's style.
- Substantial changes in content, e.g., new results, corrected values, title and authorship are not allowed without the approval of the responsible editor. In such a case, please contact the Editorial Office and return his/her consent together with the proof.
- If we do not receive your corrections **within 48 hours**, we will send you a reminder.
- Your article will be published **Online First** approximately one week after receipt of your corrected proofs. This is the **official first publication** citable with the DOI. **Further changes are, therefore, not possible.**
- The **printed version** will follow in a forthcoming issue.

### Please note

After online publication, subscribers (personal/institutional) to this journal will have access to the complete article via the DOI using the URL:

<http://dx.doi.org/10.1007/s10346-014-0498-5>

If you would like to know when your article has been published online, take advantage of our free alert service. For registration and further information, go to:

<http://www.link.springer.com>.

Due to the electronic nature of the procedure, the manuscript and the original figures will only be returned to you on special request. When you return your corrections, please inform us, if you would like to have these documents returned.

**Metadata of the article that will be visualized in OnlineFirst**

1	Article Title	<b>Geomechanical assessment of the Corvara earthflow through numerical modelling and inverse analysis</b>
2	Article Sub- Title	
3	Article Copyright - Year	<b>Springer-Verlag Berlin Heidelberg 2014 (This will be the copyright line in the final PDF)</b>
4	Journal Name	Landslides
5	Family Name	<b>Borgatti</b>
6	Particle	
7	Given Name	<b>L.</b>
8	Suffix	
9	Corresponding Author	Organization <a href="#">University of Bologna</a>
10		Division Department of Civil, Chemical, Environmental and Materials Engineering DICAM, <del>ALMA MATER STUDIORUM</del>
11	Address	Viale Risorgimento 2, Bologna 40136, Italy
12	e-mail	<a href="mailto:lisa.borgatti@unibo.it">lisa.borgatti@unibo.it</a>
13	Family Name	<b>Schädler</b>
14	Particle	
15	Given Name	<b>W.</b>
16	Suffix	
17	Author	Organization WPW Geoconsult Südwest GmbH
18		Division
19	Address	Erzbergerstraße 19, Mannheim 68165, Germany
20	e-mail	
21	Family Name	<b>Corsini</b>
22	Particle	
23	Given Name	<b>A.</b>
24	Suffix	
25	Author	Organization University of Modena and Reggio Emilia
26		Division Department of Chemical and Geological Sciences DSCG
27	Address	Largo Sant'Eufemia 19, Modena 41121, Italy
28	e-mail	

29		Family Name	<b>Meier</b>
30		Particle	
31		Given Name	<b>J.</b>
32	Author	Suffix	
33		Organization	Gruner AG
34		Division	
35		Address	Gellertstrasse 55, Basel 4020, Switzerland
36		e-mail	
<hr/>			
37		Family Name	<b>Ronchetti</b>
38		Particle	
39		Given Name	<b>F.</b>
40		Suffix	
41	Author	Organization	University of Modena and Reggio Emilia
42		Division	Department of Chemical and Geological Sciences DSCG
43		Address	Largo Sant'Eufemia 19, Modena 41121, Italy
44		e-mail	
<hr/>			
45		Family Name	<b>Schanz</b>
46		Particle	
47		Given Name	<b>T.</b>
48		Suffix	
49	Author	Organization	Ruhr-Universität Bochum
50		Division	Foundation Engineering, Soil and Rock Mechanics, Faculty of Civil and Environmental Engineering
51		Address	Building IC 5, Universitätsstrasse 150, Bochum 44780, Germany
52		e-mail	
<hr/>			
53		Received	30 April 2013
54	Schedule	Revised	
55		Accepted	30 May 2014
<hr/>			
56	Abstract	This research proposes a conceptual approach for analysis and numerical modelling of the hydromechanical behaviour of large landslides, applied to one of the source areas of the Corvara earthflow (Dolomites, Italy). The approach consists of two steps: forward calculation and inverse analysis. For the forward calculations, the geological model of the slope considering several shear zones delimitating landslide units was developed, based on a detailed dataset of field investigation and monitoring data. A viscoplastic constitutive model was used to describe the time-dependent material behaviour, i.e. the creep, of the shear	

zones. The transient distribution of pore water pressure in the slope was considered by means of an additional purely hydrogeological model. These results were used as averaged hydraulic boundary conditions in the calculation of stress and deformation fields with the continuum finite element method (FEM). The numerical model was then calibrated against ground surface displacement rates measured by D-GPS, by iteratively varying the material parameters of the shear zones. For this task, an inverse analysis concept was applied, based on statistical analyses and an evolutionary optimisation algorithm. The inverse modelling strategy was further applied to gather statistical information on model behaviour, on the sensitivity of model parameters and on the quality of the obtained calibration. Results show that the calibrated model was able to appropriately simulate the displacement field of the earthflow and allow the requirements, difficulties and problems, as well as the advantages and benefits of the proposed numerical modelling concept to be highlighted.

---

57	Keywords separated by ' - '	Finite element method - Numerical modelling - Corvara earthflow - Dolomites - Italy
58	Foot note information	

---

Landslides

DOI 10.1007/s10346-014-0498-5

Received: 30 April 2013

Accepted: 30 May 2014

© Springer-Verlag Berlin Heidelberg 2014

W. Schädler · L. Borgatti · A. Corsini · J. Meier · F. Ronchetti · T. Schanz

## Geomechanical assessment of the Corvara earthflow through numerical modelling and inverse analysis

**Abstract** This research proposes a conceptual approach for analysis and numerical modelling of the hydromechanical behaviour of large landslides, applied to one of the source areas of the Corvara earthflow (Dolomites, Italy). The approach consists of two steps: forward calculation and inverse analysis. For the forward calculations, the geological model of the slope considering several shear zones delimitating landslide units was developed, based on a detailed dataset of field investigation and monitoring data. A viscoplastic constitutive model was used to describe the time-dependent material behaviour, i.e. the creep, of the shear zones. The transient distribution of pore water pressure in the slope was considered by means of an additional purely hydrogeological model. These results were used as averaged hydraulic boundary conditions in the calculation of stress and deformation fields with the continuum finite element method (FEM). The numerical model was then calibrated against ground surface displacement rates measured by D-GPS, by iteratively varying the material parameters of the shear zones. For this task, an inverse analysis concept was applied, based on statistical analyses and an evolutionary optimisation algorithm. The inverse modelling strategy was further applied to gather statistical information on model behaviour, on the sensitivity of model parameters and on the quality of the obtained calibration. Results show that the calibrated model was able to appropriately simulate the displacement field of the earthflow and allow the requirements, difficulties and problems, as well as the advantages and benefits of the proposed numerical modelling concept to be highlighted.

**Keywords** Finite element method · Numerical modelling · Corvara earthflow · Dolomites · Italy

### Introduction

In Italy, a number of large-scale and deep-seated complex landslides, including earthflows, affect the Alps and the Apennines (Guzzetti et al. 1994; Trigila et al. 2010). They can be up to 50 m deep and can cover several square kilometres. In the affected regions, this represents a major socio-economic problem, as landslides may cause continuous damage to infrastructures and, in several cases, they pose a potential threat to settlements.

Since few decades, numerical modelling has been applied to earthflows by various authors using different approaches, with the aim of better understanding landslide evolution (Picarelli et al. 1995; Angeli et al. 1996a, b, 1998; Vulliet and Bonnard 1996; van Asch et al. 2007; Comegna et al. 2007). In some case, the objective of the numerical modelling was to assist the design of effective technical countermeasures (Borgatti et al. 2007a; Marcato et al. 2009, 2012).

A manual trial-and-error procedure is often adopted to calibrate the numerical slope model against observed displacements. Alongside this approach, which is strongly based on expert knowledge, the application of inverse analyses for the calibration of numerical models is an appropriate concept for the identification of parameters that cannot be easily determined directly from

laboratory experiments (Hvorslev 1949). Inverse analysis is widely used in many engineering fields such as hydraulics, damage analysis and structural dynamics. A variety of different optimisation schemes and algorithms are available from literature. In recent years, due to the availability of faster computer hardware, inverse parameter identification strategies and optimisation procedures have been more and more frequently used also in engineering geology and geomechanics by many authors (Gens et al. 1996; Ledesma et al. 1996a, b; Zhang et al. 2003; Calvello and Finno 2004; Malecot et al. 2004; Feng et al. 2006; Finsterle 2006; Meier et al. 2006; Lefvasseur et al. 2008; Meier 2008; Meier et al. 2008).

In this paper, a method for modelling the hydromechanical behaviour of large landslides is presented and applied to a source area of the Corvara earthflow in the Dolomites, Italy. This case study is relevant, as an acceleration of the landslide could determine the involvement of a part of the village, the damming of the side flank streams and the disruption of the national road running on the accumulation area.

The method consists of two parts: forward calculations and inverse analysis. In order to perform forward calculations using a continuum mechanical approach with the finite element method, different model components have to be implemented. The geological model describes the source area, and an adequate constitutive model takes into consideration weight, strength and stiffness of units and layers. In particular, a creep model describes the time-dependent behaviour of the material forming the shear zones. Additionally, a hydrogeological model describing the transient distribution of pore water pressures is used to approximate the hydraulic boundary conditions. In order to derive the parameters which yield a good simulation of reality, the finite element (FE) model is calibrated against displacement rates measured in the field, by iteratively varying the material parameters of the shear zones. For this task, the inverse parameter identification technique of Schanz et al. (2006), Schanz and Meier (2008) and Meier et al. (2008) is applied. The technique is based on statistical analyses and appropriate optimisation algorithms, which have been adapted and tested especially for geotechnical applications. Based on the Corvara case study, the requirements, difficulties and problems as well as the advantages and benefits of the proposed numerical modelling concept are highlighted.

### The Corvara landslide

#### Setting of the landslide area

Located in a renowned tourist area in the Dolomites of Italy, the Corvara landslide (Fig. 1) was selected for this study on the basis of its socio-economic relevance and for the availability of an extensive dataset of field investigation and monitoring data.

The landslide area extends from Corvara in Badiato Pralongià, from about 1,600 to 2,100 m a.s.l. The landslide can be described as an active slow-moving earthflow with an estimated volume of 30 million m<sup>3</sup>. It damages a national road and a set of facilities

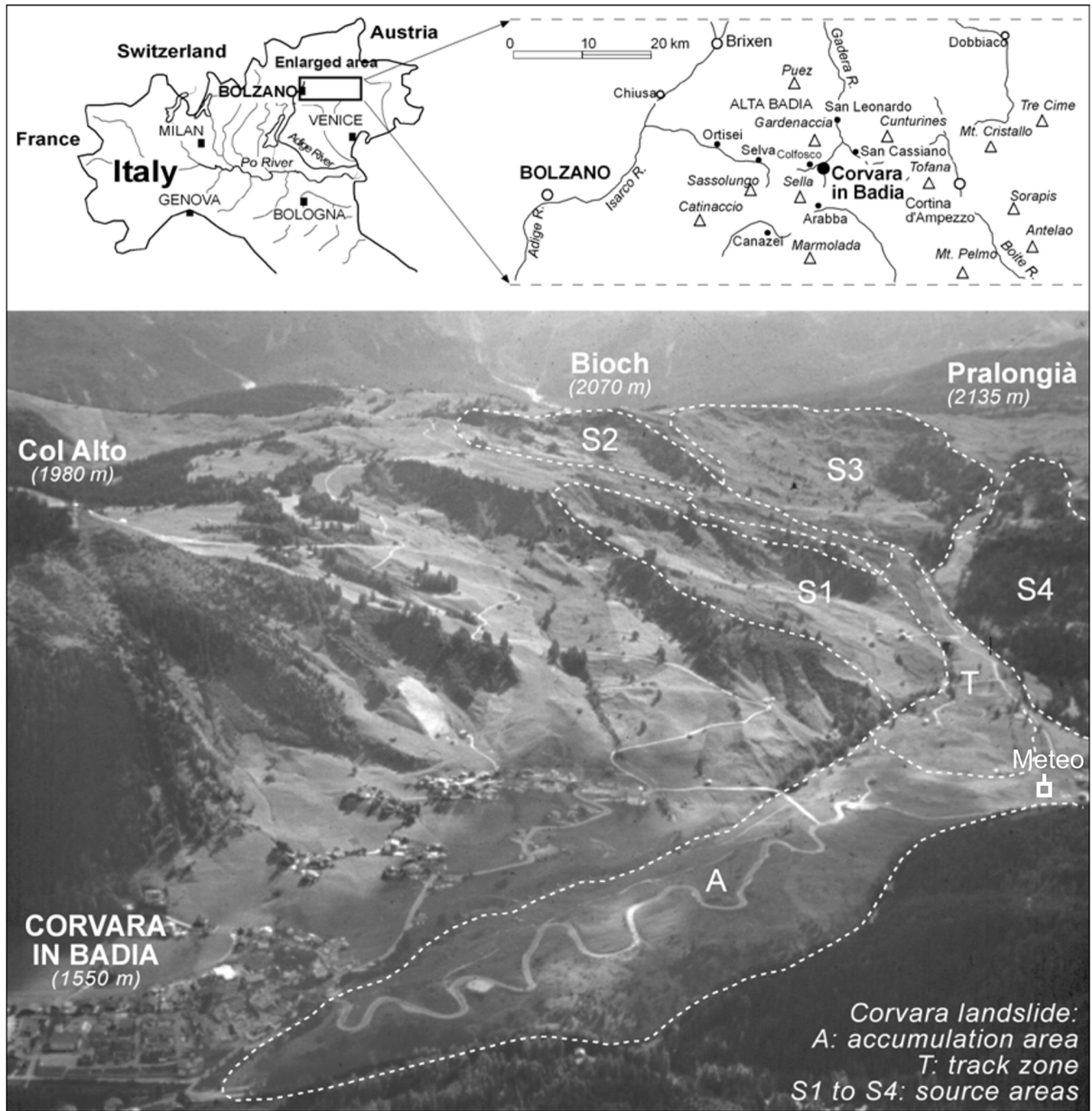


**Fig. 1** Location and overview of the Corvara earthflow

113 including ski infrastructures, electricity lines and a golf course. In  
 114 the worst-case scenario, the landslide might accelerate and affect  
 115 some buildings located at its toe and possibly endanger down-  
 116 stream settlements by damming the torrents running at its flanks.  
 117 For this reason, geological, geomorphologic and geotechnical anal-  
 118 yses of the landslide have been carried out since 1996 with the  
 119 support of the autonomous province of Bolzano—South Tyrol,  
 120 together with the Corvara municipality (Corsini et al. 2001; Soldati  
 121 et al. 2004; Corsini et al. 2005; Panizza et al. 2006; Borgatti et al.  
 122 2007b; Borgatti and Soldati 2010).

Bedrock of the landslide site is mostly composed of Tri- 123  
 assic flysch-type rock masses, La Valle and San Cassiano 124  
 units, which consist of an alternation of volcano-clastic 125  
 sandstones, marly limestones and clay shales. The ratio of 126  
 hard to soft rocks varies from 1 to more than 2 (Corsini et 127  
 al. 2005). Bedrock forms a monocline dipping upslope at 128  
 about 30° of inclination, and shows three to four major 129  
 tectonic joint sets generated during the Alpine orogen 130  
 (Corsini 2000). The overall geomorphologic setting of the 131  
 slope is primarily controlled by the attitude of bedding and 132

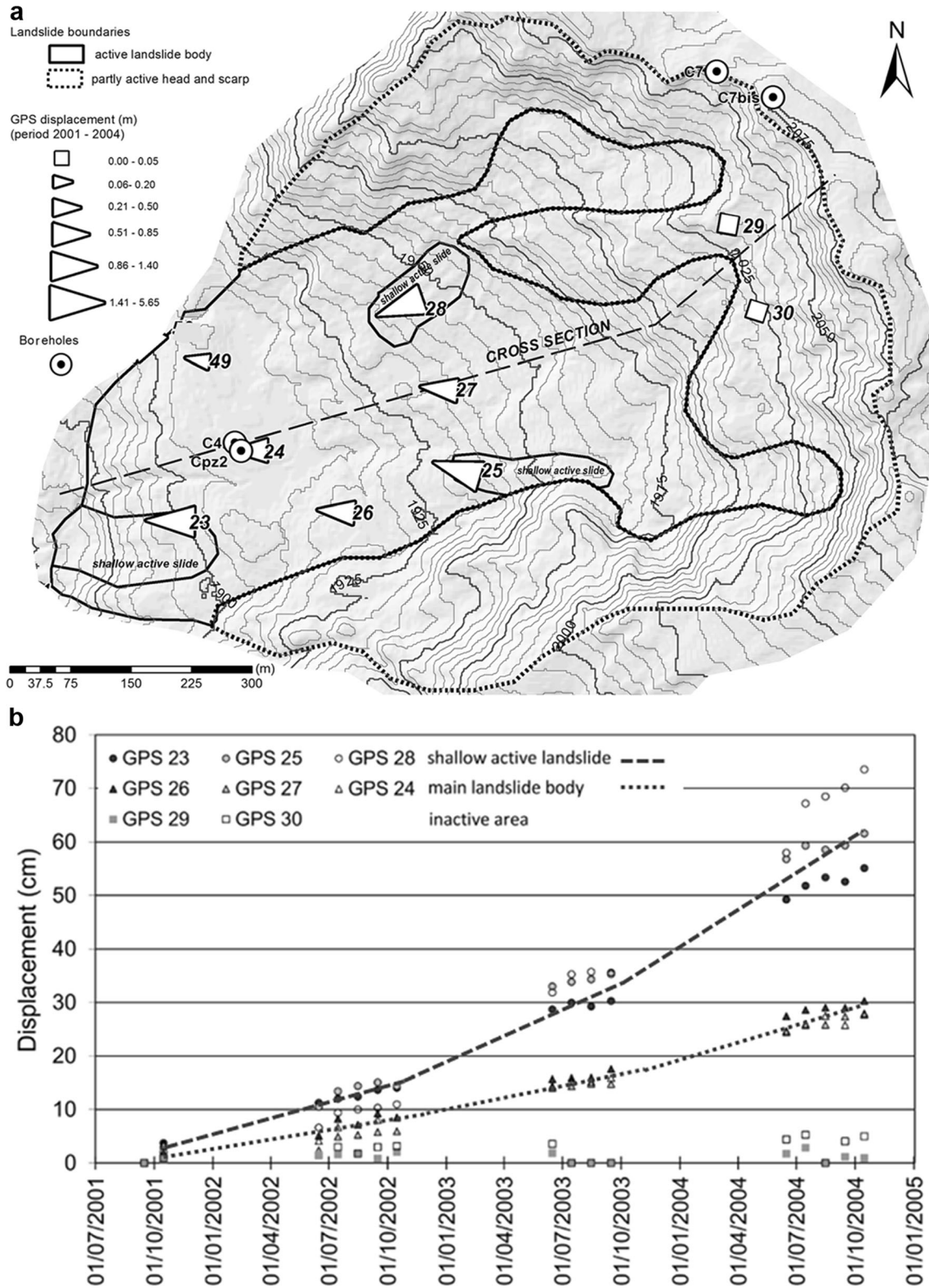


**Fig. 2** Displacement vectors (a) and displacements (b) measured in source area S3 between 2001 and 2004 (GPS data from Panizza et al. 2006). Benchmark 49 was measured starting from 2003; vector has been scaled up respectively. Location of boreholes and of cross section of Fig. 5 is also reported (a)

133 joints and, secondarily, by the action of Pleistocene glaciers  
 134 and of Holocene weathering and mass wasting processes  
 135 (Corsini et al. 1999; Corsini 2000).

At present, in the Corvara landslide, distinct source (S), track  
 (T) and accumulation (A) areas can be outlined. The source area  
 itself can be subdivided into four sectors (S<sub>1</sub>, S<sub>2</sub>, S<sub>3</sub> and S<sub>4</sub> in

136  
 137  
 138

139 Fig. 1). Observations made on borehole cores, radiocarbon data  
 140 and historical archives point to a long-term landslide evolution  
 141 characterised by periods of increased activity during which the  
 142 main scarp probably retrogressed, the accumulation zone grew  
 143 and the earthflow foot advanced down the valley (Corsini et al.  
 144 2005; Panizza et al. 2006).

145 In the period 2001–2004, movements in the source area were  
 146 “very slow” to “slow” (following Cruden and Varnes 1996), ranging  
 147 from 50 to 1,000 mm/year, with acceleration phases taking place  
 148 mainly in autumn and late spring, after prolonged rainfall and/or  
 149 snowmelt events. Hence, surges can be expected in the scenarios of  
 150 extreme meteorological events and/or of excess pore pressure  
 151 build-up due to activation of local shallow earthflows. This would  
 152 imply a large amount of material to reach the track zone, with  
 153 eventual total reactivation of the Corvara landslide and subse-  
 154 quent large damage. For this reasons, displacement rates in source  
 155 area S3 have been monitored by RTK D-GPS during 15 monitoring  
 156 campaigns carried out four to five times a year in the period from  
 157 2001 to 2004. Two master stations were set in stable areas outside  
 158 the landslide. The displacement history of benchmarks 23–30 is  
 159 plotted in Fig. 2, showing the norms of 3D displacement vectors for  
 160 each measurement date and their directions. The gap periods of  
 161 10 months in the records are partly due to the existence of a thick  
 162 snow cover in winter and spring seasons, during which measure-  
 163 ments were not possible but significant displacements occurred.  
 164 The data exhibit approximately linear trends. Rates of around  
 165 0.1 m/year were measured at benchmarks 24, 26 and 27, lying on  
 166 the main landslide body of source area S3. Significantly higher  
 167 displacement rates of around 0.2 m/year were observed in areas  
 168 where, in addition to the movement of the main landslide body,  
 169 the slope is also affected by shallow landslides (GPS benchmarks  
 170 23, 25 and 28). The GPS benchmarks 29 and 30, located in a  
 171 relatively stable area below the crest of the slope and above the  
 172 active part of source area S3, did not show significant displace-  
 173 ments (Fig. 2).

174 **Geological model of source area S3**

175 A geological and geotechnical model of the whole Corvara land-  
 176 slide was made available by Panizza et al. (2006), including surface  
 177 topography, stratigraphic profile, depth of sliding zones and di-  
 178 mensions of landslide bodies characterised by different displace-  
 179 ment rates.

180 Surface topography was obtained by profiling a DEM produced  
 181 in 2005 by the autonomous province of Bolzano using airborne  
 182 LiDAR. Its nominal elevation accuracy is in the order of 1 m. A  
 183 large number of geotechnical laboratory tests were carried out on  
 184 samples of the landslide body in order to characterise the mate-  
 185 rials (grain size distribution, Atterberg limits, etc. on 25 soil sam-  
 186 ples, see Panizza et al. 2006) and assess shear strength (direct shear  
 187 tests on 5 samples, see Panizza et al. 2006). Stiffness under differ-  
 188 ent stress loads, consolidation behaviour and oedometer creep  
 189 behaviour was analysed with oedometer tests, also with prolonged  
 190 creep phases, isotropic compression and deviatoric creep tests  
 191 (Schädler 2008). The landslide body is made up of a normally  
 192 consolidated soil matrix of silty clays and clayey silts, which  
 193 encloses coarser components, such as a variety of angular gravel-  
 194 size particles, up to rock blocks. These consist of volcanoclastic  
 195 and calcareous sandstones, marly limestones or dolostones. The  
 196 mechanical behaviour of the shear zones is assumed to be mainly

controlled by the properties of the clay-rich soil matrix 197  
 (Table 1). 198

199 Underground boundaries, including the depth of sliding sur-  
 200 faces, have been obtained by interpreting field evidence, borehole  
 201 stratigraphy, geoelectric and seismic refraction data, and inclinom-  
 202 eter measurements. In source area S3, according to inclinometer  
 203 C4 (Fig. 2), the landslide body is prevalently moving along a basal  
 204 shear zone 40 m deep (Fig. 3). From inclinometer and TDR cables  
 205 measurements, it can be inferred that the thickness of the main  
 206 shear zones is in the order of 1 to 2 m (Corsini et al. 2005). In the  
 207 lower part of source area S3, field evidence suggests that the  
 208 landslide body thins out to a few metres due to the presence of a  
 209 buried bedrock ridge. In the geological model, the basal surface of  
 210 rupture of source area S3 is slightly dipping upslope in the foot  
 211 area and outcropping upslope the track zone. In some sectors, a  
 212 hummocky morphology and the presence of lateral ridges indicate  
 213 that shallow earthflows are locally active over secondary shear  
 214 zones, 3 to 10 m deep.

215 Below the main shear zone, old landslide material, colluvium  
 216 and bedrock were found in borehole core of inclinometer C4.  
 217 Since these materials gave very similar responses during the geo-  
 218 physical soundings (Panizza et al. 2006) and inclinometer C4  
 219 showed no movements below 40-m depth, when assigning prop-  
 220 erties to the different parts of the geological model, these materials  
 221 were treated as one single unit (Fig. 3). Concerning  
 222 hydrogeological conditions, two open pipe piezometers (in bore-  
 223 holes Cp22 and C7) and one unsealed and uncemented inclinom-  
 224 eter case operating as open pipe piezometer (C4) lie in source area  
 225 S3 (Fig. 2, Table 2).

226 Measurement series recorded by electric transducers equipped  
 227 with data loggers (acquisition time set to 30 min) indicated a ground-  
 228 water depth varying from 0 to 8 m in the period 2001–2004 and  
 229 revealed the existence of two different types of overlapping ground-  
 230 water regimes. The first is connected to streams, ponds and marshes  
 231 and therefore shows relatively small variations (C4 in Fig. 4); the  
 232 second is linked to the infiltration of rainfall and consequently  
 233 undergoes much larger seasonal fluctuations (Cp22 in Fig. 4). In  
 234 order to model the hydrogeological conditions for the entire 2D  
 235 slope model, a single continuous aquifer marked by one average  
 236 groundwater depth of 1 m was initially idealised. The geological and  
 237 hydrogeological model of the slope is shown in Fig. 5.

238 **Inverse parameter identification technique**

239 Instead of varying the model parameters in a conventional, man-  
 240 ual trial-and-error procedure, an inverse parameter identification  
 241 approach using the back analysis method (Cividini et al. 1981) was  
 242 applied to calibrate the numerical model of the slope and to back-  
 243 calculate a subset of material parameters for which the available  
 244 field measurements indicate a high sensitivity. The identification  
 245 approach consists of a procedure performed in several substeps  
 246 during which parameters are iteratively changed to achieve better  
 247 fit between the model results and the field measurements. Good-  
 248 ness of fit is measured by the objective function  $f(x)$ , which has to  
 249 be defined individually for each specific back-calculation task. The  
 250 objective function used here is the mean-square deviation between  
 251 monitoring data and simulation results. In order to confine the  
 252 best fit searching procedure to reasonable solutions in physical  
 253 and engineering terms, a bounded parameter search space  $\Omega$  is  
 254 defined.

**Q3.1 Table 1** Average geotechnical parameters of the landslide material from source area

Parameter	Value
Unit weight $\gamma$	15–22 kN/m <sup>3</sup>
Sand fraction	15 %
Silt fraction	50 %
Clay fraction	35 %
Lime content	39.7–55.5 %
Plasticity index	10–30 %
Natural water content	20–45 %
Plasticity Chart	MH-OH, ML-OL
Undrained cohesion $c_u$	30–100 kN/m <sup>2</sup>
Effective peak friction angle $\phi^*$	20–30°
Effective peak cohesion $c'$	10–35 kN/m <sup>2</sup>
Residual friction angle $\phi_r$	15–20°
Modified compression index $\lambda^*$	0.050–0.064
Modified swelling index $\kappa^*$	0.020–0.035
Modified creep index $\mu^*$	$8.09 \times 10^{-4}$ – $1.46 \times 10^{-3}$
Permeability $k$	$2.10 \times 10^{-10}$ m/s
Oedometer modulus $E$	5–53 MN/m <sup>2</sup>
Shear modulus $G$	5,560 kN/m <sup>2</sup>
Poisson's ratio $\nu$	0.35

From Corsini et al. (2005), Panizza et al. (2006), and Schädler (2008)

In this work, the solution of the optimisation problem (i.e., minimisation of the objective function) is based on a strategy called Shuffled Complex Evolutionary algorithm (SCE)

proposed by Duan et al. (1992, 1993, 1994). The SCE belongs to a group of algorithms that combine methods and strategies of different optimisation algorithms in order to overcome weak points, restrictions and disadvantages of the individual methods when used alone. Prior to the application of an optimisation scheme to a back-calculation problem, it is highly recommended to gain more information on the initially unknown objective function topology. For this purpose, a number of forward calculations are performed using randomly chosen parameter sets within physically reasonable ranges, and the objective function value is calculated for each parameter set. To visualise this kind of multi-dimensional data, a scatter-plot matrix as shown in Fig. 6a is often used. In this type of scatter-plot matrix, each row and column correspond to one parameter being varied, where each subplot can be interpreted as projection of the multi-dimensional objective function topology (Manly 1944). To avoid appending an additional row to the matrix showing the objective function value on its vertical axis, these plots are moved to the diagonal elements of the plot matrix. For each forward calculation of the randomly chosen parameter sets, one data point can be plotted in each of the subplots of a scatter-plot matrix. To allow for an assessment of the distribution of a certain objective function value range, a filtered subset of the randomly chosen parameter sets is usually plotted. If only the best items are plotted, the resulting point clouds give an impression of the optimal objective function value range.

For example, a simple analytical function is used for generating the scatter-plot matrix of Fig. 6, where only parameter sets are shown leading to  $f(x) \leq 0.5$  (10,000 parameter sets had been calculated within  $-1 \leq x_{1,2,3} \leq +1$  of which 281 sets satisfy  $f(x) \leq 0.5$ ). The three columns and rows of Fig. 6a correspond to the parameters  $x_1$ ,  $x_2$  and  $x_3$  of the objective function. As visible from Fig. 6b, the optimal value range envelopes show a “correlation” between  $x_1$  and  $x_3$ . Additionally, from the analytical function, it is to be

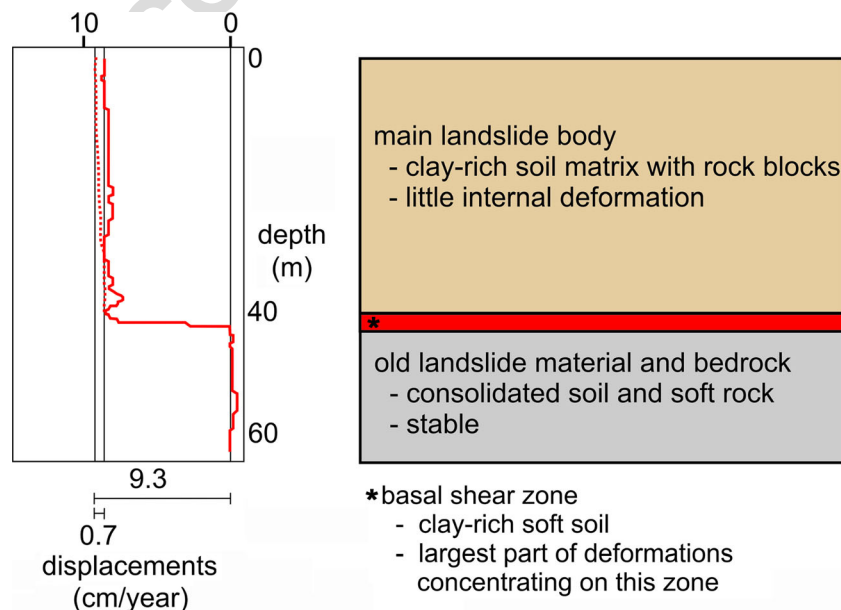


**Fig. 3** Internal stratification of the geological model (inclinometer data from Corsini et al. 2005 and Panizza et al. 2006). Solid red line indicates inclinometric profile and layering observed along the entire length of the tube; dotted red line indicates inclinometric profile after the rupture of the tube at 40-m depth

t2.1 **Table 2** Groundwater monitoring devices

t2.2	Label	Diameter (inch)	Depth (m)	Type
t2.3	C4	2	60	Unsealed/uncemented inclinometer case operating as open pipe piezometer
t2.4	Cpz2	2	45	Open pipe piezometer fissured only at 39–45-m depth
	C7	4	88	Open pipe piezometer

293 expected that  $x_1$  is the least and  $x_3$  is the most sensitive parameter  
 294 for  $f(x)$ . The following statements hold:

- 295 – The projected shapes of the isosurfaces for  $f(x)=0.5$  of Fig. 6b  
 296 correspond very well to the envelopes of the point clouds of the  
 297 individual subplots of Fig. 6a.
- 298 – The correlation of  $x_1$  and  $x_3$  is nicely visible in the correspond-  
 299 ing subplots and for the point cloud shown; a 2D linear correla-  
 300 tion coefficient of  $-0.74$  is calculated. As to be expected, for  
 301 the other parameter combinations, no correlation is visible.
- 302 – The diagonal elements of the scatter-plot matrix provide  
 303 insight to the local sensitivity of the objective function range  
 304 shown for  $x_1$ ,  $x_2$  and  $x_3$ . First, only one lower tip of the point  
 305 cloud envelope is visible, what indicates that only one opti-  
 306 mum is existing within the investigated range. Second, as more  
 307 sensitive a parameter is, as more “pointy” the lower tip of the  
 308 point cloud envelope should be. As expected,  $x_1$  is the least and  
 309  $x_3$  is the most sensitive parameter. In general, if an inverse  
 310 problem is well posed, each of the diagonal plots should

present one firm extreme value. Otherwise, the respective pa- 311  
 parameter may not be identified reliably. 312

- The diagonal elements of the scatter-plot matrix indicate 313  
 that the global optimum is somewhere near  $x_1=0$ ,  $x_2=0$  314  
 and  $x_3=0$ . 315  
 316

This kind of statistical analysis of the results of forward calcula- 317  
 tions can be used to determine those parameters which are 318  
 indifferent to the system response or dependent on each other. 319  
 These parameters can be removed prior to back-calculation. Fur- 320  
 thermore, the remaining parameters can be classified according to 321  
 their influence (Schwarz 2001). 322

### Forward calculations 323

### Hydrogeological model 324

Steady state and transient groundwater flow calculations were 325  
 carried out applying the FE code SEEP/W (Krahn 2004). Zero flow 326

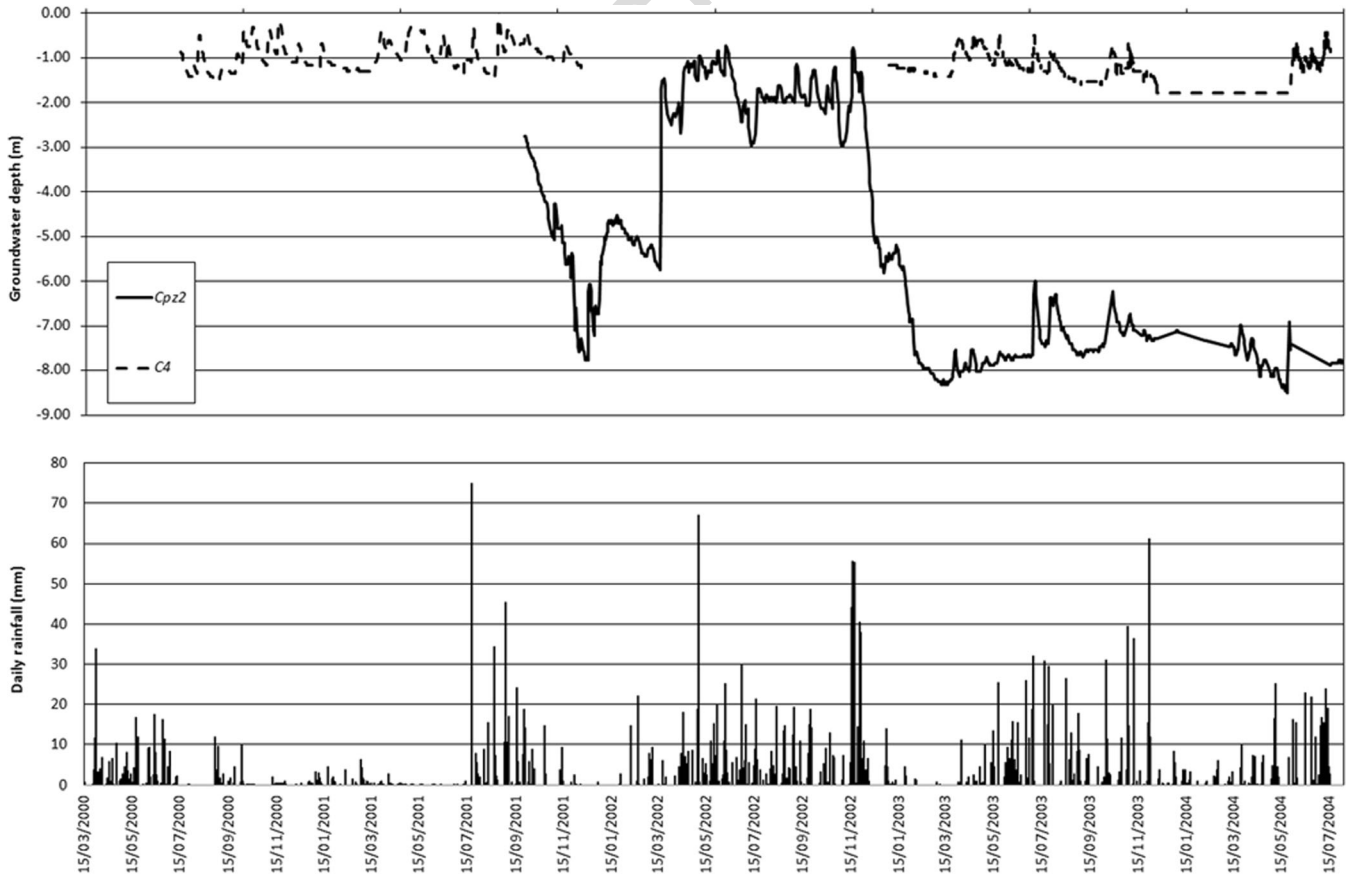


**Fig. 4** Piezometric data and rainfall during 2001–2004 monitoring period

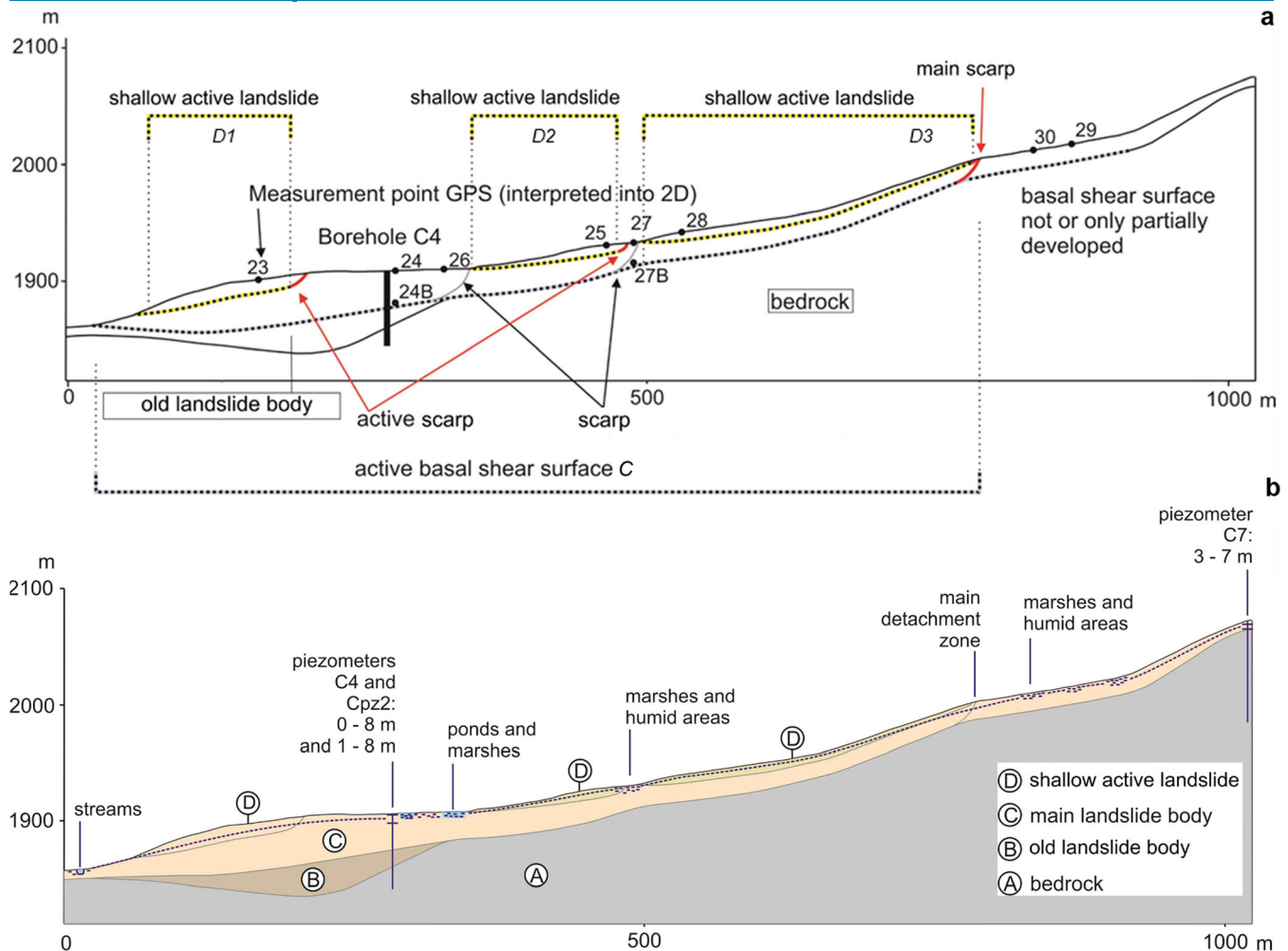


**Fig. 5** a 2D geological model of source area S3. See Fig. 2 for location. Point 24B is based on inclinometric measurements. b Simplified hydrogeological model assuming an average water table to be implemented in the seepage model (piezometer data from Panizza et al. 2006)

327 was allowed through the basal boundary of the geological model, 328 and fixed groundwater heads were prescribed at its lateral bound- 329 aries based on monitoring data. Water levels were then gener- 330 ated by means of a 2D slope infiltration and seepage model. Input flow 331 rate was calculated monthly according to the Thornthwaite (1948) 332 formula, using rainfall, snowmelt and temperature data recorded 333 at the on-site meteorological station (observation period 2001– 334 2004, Table 3).

335 The calculated effective recharge was simulated using a trans- 336 ient flux boundary condition applied at each node on the slope 337 surface profile ( $q$  in m/s, see Krahn 2004). At every node, the 338 potential seepage review boundary condition was adopted in 339 order to avoid ponding. A null-flux condition was imposed at 340 the base of the model and at the upslope model boundary 341 because the crest of the slope was assumed to represent the 342 main water divide. The model parameters (saturated and unsat- 343 urated hydraulic conductivities, volumetric water content func- 344 tions and conductivity functions, here represented by a straight 345 line) were estimated from grain-size distributions, Atterberg 346 limits, water content at saturation and coefficient of volume 347 compressibility of the landslide materials. Recommendations 348 within Krahn (2004) and data proposed by other authors (e.g.

349 Caris and van Asch 1991; Bonomi and Cavallin 1999; Malet et al. 350 2005; Tacher et al. 2005; Francois et al. 2007) were also consid- 351 ered. In order to further simplify the hydrogeological model, 352 isotropic hydraulic permeability was assumed for all materials, 353 except for shallow landslide bodies in which the vertical perme- 354 ability was assumed to be three times higher than the horizontal 355 one (Table 4).

356 The infiltration and seepage model was calibrated by a trial- 357 and-error procedure against the monitoring data of piezometer 358 Cpz2, in which groundwater level is largely controlled by infiltra- 359 tion (Fig. 4). Calibration was continued until an acceptable fit 360 between calculated and measured level was obtained for the re- 361 charge as well as for the discharge curve (Fig. 7). Conservative 362 hydrostatic pore pressure distributions were then used in the 363 deformation model.

**Finite element hydraulic-mechanical model** 364

365 The kinematics of the slope during the observation period (2001– 366 2004) were simulated using the FE method. All calculations were 367 carried out using the Plaxiscode version 8.2 (2003), taking into 368 account the effect of large deformations by means of an updated 369 Lagrangian formulation (updated mesh analysis). Calculations

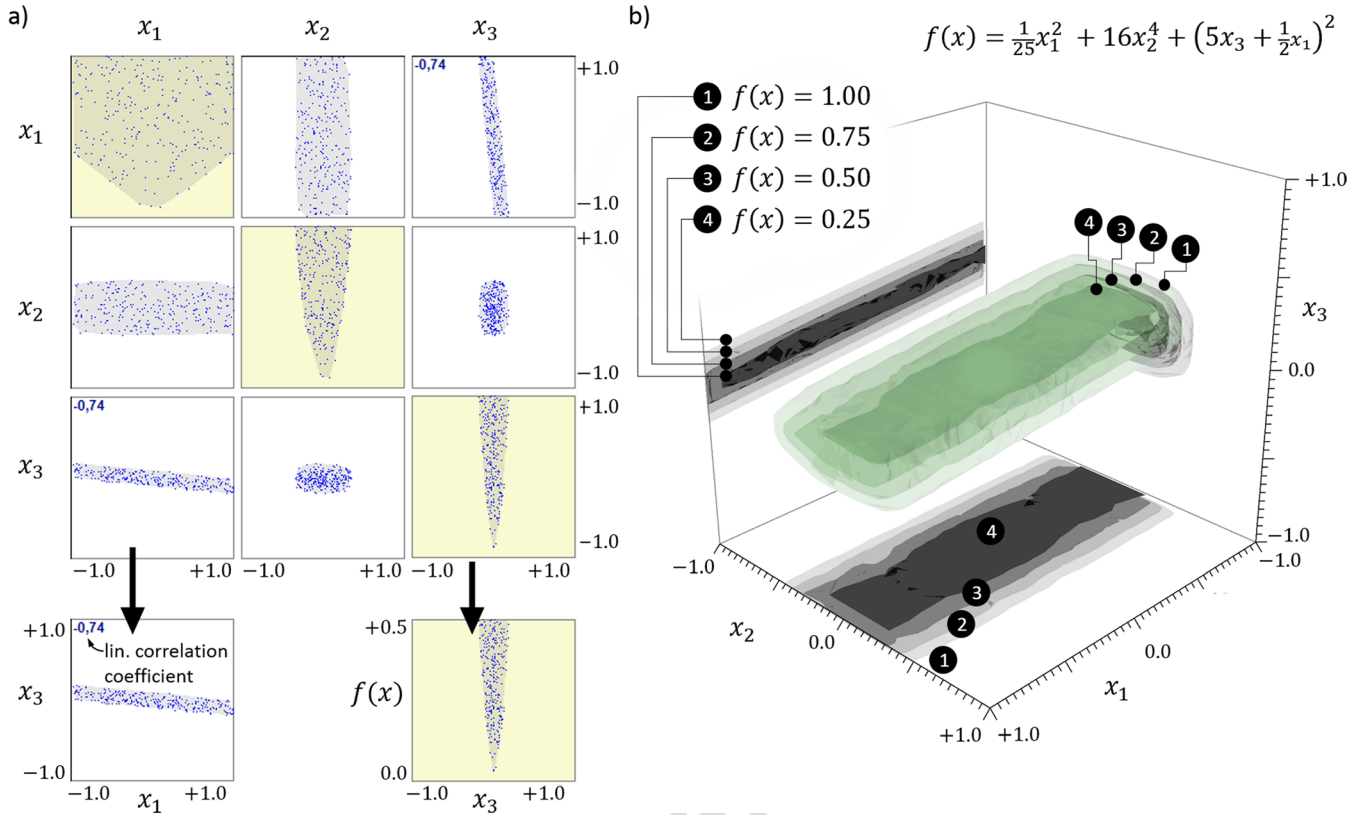


**Fig. 6** Scheme of the scatter-plot matrix. **a** Multi-dimensional data plotted in a scatter-plot matrix. **b** Example of the objective function calculation for a simple analytical function

370 were performed as consolidation analyses, i.e. modelling the  
 371 stress-strain field and taking into account the time-dependent  
 372 development of pore pressures. A plane-strain geometrical config-  
 373 uration with the real dimensions of the slope was used. The model  
 374 was discretised using 2790 triangular 15-node elements. Horizontal

deformation fixities were assigned to the lateral boundaries and  
 total deformation fixities to the basal boundary.

Based on lab tests (Table 1) and on the results of calibration of  
 the constitutive model (Schädler 2008), the soil along the shear  
 zones can be regarded as a plastic material, which is characterised

375  
 376  
 377  
 378  
 379

t3.1 **Table 3** Average climatic data for the observation period. The calculated effective recharge was used as input in the infiltration and seepage model

Month	Mean monthly air temperature (°C)	Mean monthly rainfall (mm)	Mean monthly snowmelt (mm)	Mean monthly evapotranspiration (mm)	Mean monthly effective recharge (mm)
Jan	-4.7	29.0	0.0	0.8	28.1
Feb	-3.1	29.1	10.3	1.1	38.4
Mar	0.5	46.8	22.9	7.4	62.3
Apr	2.7	54.1	6.1	30.1	30.1
May	8.3	92.5	0.0	92.5	0.0
June	12.4	82.4	0.0	82.4	0.0
July	13.4	97.9	0.0	97.9	0.0
Aug	14.1	75.9	0.0	75.9	0.0
Sept	9.0	80.5	0.0	80.5	0.0
Oct	5.4	69.8	0.0	50.6	19.1
Nov	0.8	149.6	11.0	4.9	155.8
Dec	-2.5	39.1	20.3	1.1	58.3
Total		846.6	70.7	524.5	392.2

t3.2  
 t3.3  
 t3.4  
 t3.5  
 t3.6  
 t3.7  
 t3.8  
 t3.9  
 t3.10  
 t3.11  
 t3.12  
 t3.13  
 t3.14

t4.1 **Table 4** Saturated hydraulic conductivity values used in the trial-and-error procedure for the calibration of the steady-state groundwater flow calculation

Layer	Fixed values and constraints (m/day)	Calibrated values (m/day)	Adopted values (m/s)
D	Active shallow landslide bodies	$D_2 > D_1; < 0.09$	3.47E-07
		$D_1 \geq C$	1.16E-07
C	Main landslide body	0.009	1.04E-07
B	Old landslide body	$A < B < C$	4.63E-08
A	Bedrock	0.0009	1.04E-08

$D_1$  horizontal,  $D_2$  vertical

380 by a pronounced time-dependent behaviour (Picarelli et al. 2000;  
 381 Augustesen et al. 2004). Therefore, the Soft Soil Creep model was  
 382 used as a constitutive model for these zones (Vermeer and Neher  
 383 1999). A set of three parameters (effective cohesion  $c$ , effective  
 384 friction angle  $\varphi$  and dilatancy angle  $\psi$ ) is required to model failure  
 385 according to the Mohr-Coulomb criterion. Two further parameters  
 386 are used to model the amount of plastic and elastic strains and their  
 387 stress dependency. The modified compression index ( $\lambda^*$ ) represents  
 388 the slope of the normal consolidation line. The modified swelling  
 389 index ( $\kappa^*$ ) is related to the unloading or swelling line. The modified  
 390 creep index ( $\mu^*$ ) measures the development of volumetric creep  
 391 deformations with the logarithm of time.

392 Due to the age of the landslide activity in source area  $S_3$  and the  
 393 continuous nature of the sliding processes, it was assumed that in  
 394 the long term, the shear zones have undergone relative displacements  
 395 in the range of at least tens of metres. Therefore, the material of the  
 396 shear zones is assumed to have reached the residual strength. As the  
 397 subsoil away from the shear zones shows little internal deformations  
 398 (Fig. 3), the material behaviour was modelled as linear-elastic to  
 399 account for the gravitational loads that these materials exert onto  
 400 the shear-zone layers.

401 The initial stress state at the beginning of the modelled time  
 402 span, i.e. in the year 2001, is mainly a consequence of the long-  
 403 term history of the slope. Therefore, the initial stress state in the  
 404 model was generated by simulating a simplified loading history,

based on the knowledge about the slope evolution. Modelling of  
 the different phases was performed in six phases: gravity loading,  
 unloading by weathering and erosion, loading by glaciers, forma-  
 tion of weak zones, unloading after glaciation and creeping. It was  
 assumed that already prior to the last glaciation, the slope was  
 characterised by a gently inclined profile. Therefore, in a first  
 calculation phase, a stress field was created by gravity loading  
 based on the actual topography and assuming a homogeneous  
 linear elastic material, whose specific weight equals that attributed  
 to the actual bedrock. During gravity loading, Poisson's ratio was  
 adjusted to result in a ratio between horizontal and vertical stress-  
 es corresponding approximately to a  $K_0$  value of 0.8. Then, the  
 value of Poisson's ratio was changed to the assumed current value  
 (0.33), which was then used in further calculation phases. In a  
 second calculation phase, the slope model was unloaded by lower-  
 ing the specific weight of all layers, except for the bedrock, to  
 present-day values. In a third phase, a distributed load of  
 1,000 kN/m<sup>2</sup> was applied perpendicularly to the ground surface  
 to simulate loading by Pleistocene glaciers. In a fourth phase,  
 weak layers were inserted into the model as a result of deep  
 weathering during the glaciation and deglaciation phases. In a  
 fifth phase, the slope was unloaded very fast to its actual state  
 immediately after the shear-zone layers had been inserted. In  
 a sixth phase, the shear-zone materials were left creeping  
 under the assumed average water pressures until approximately  
 constant displacement rates were observed with respect to  
 the time-scale of the simulated monitoring period. The duration  
 of this phase (10,000 days, approx. 27 years) had to be defined  
 arbitrarily to comply with this criterion. The stress state reached  
 at the end of this last phase of the loading history was taken as  
 initial stress state for the simulation of deformations in the  
 monitoring period.

A first-trial forward calculation, using parameter values directly  
 from the laboratory tests, was carried out (Table 5). The calculated  
 total displacements at the end of the 3 years of the monitoring  
 period appeared to be underestimated by the model, with total  
 displacements in the order of 7 cm with respect to 30–70 cm  
 measured in the field. Anyhow, in the most active region, the  
 shape of the displacement profile and the direction of displacement  
 vectors were in qualitative agreement with the measurements.

### Inverse analysis

### Statistical analysis

The results of the first-trial calculation suggest that the material  
 parameters are not the same for all shear zones (i.e. basal shear  
 zone C and shear zones of shallow active landslides  $D_1$ ,  $D_2$  and  $D_3$ ,

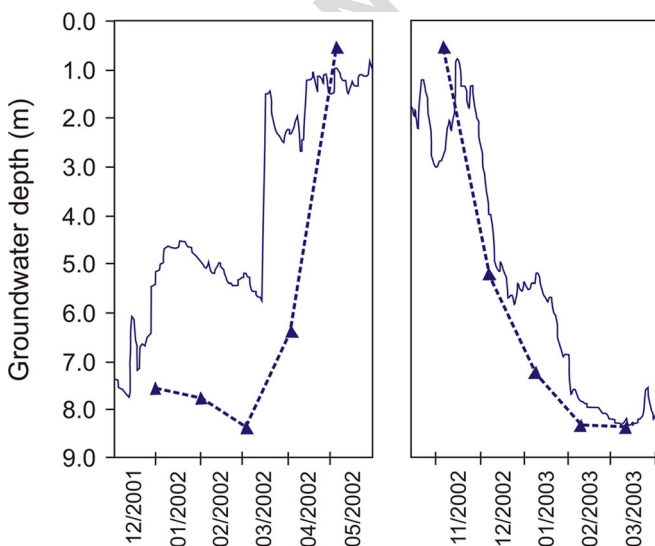


**Fig. 7** Observed and calculated groundwater depths in borehole Cpz2 from December 2001 to March 2003 during recharge and discharge phases

t5.1 **Table 5** Experimental parameter values used for all the shear zones in the first-  
 t5.2 trial forward calculation. Shear strength parameters from Panizza et al. (2006) and  
 t5.3 stiffness parameters and creep parameters by oedometer tests in Schädler (2008),  
 t5.4 as shown in Table 2

Material parameter	Value
t5.3 $\lambda^*$	0.057
t5.4 $\kappa^*$	0.028
t5.5 $\mu^*$	$1.2 \times 10^{-3}$
t5.6 $\Phi$	20°
t5.7 $c$	27 kN/m <sup>2</sup>
$\psi$	0°

see Fig. 5). Hence, in the statistical analysis of the model behaviour, some of the parameters were correlated, while others were chosen to be identified independently, trying to minimise the number of variable parameters, but not to oversimplify the model.

The displacement rates depend on shear strength and creep behaviour of the shear zones, which is in turn controlled mainly by the modified creep index  $\mu^*$  and is also related to their stress-dependent compressibility and vice versa. The latter is described by the modified compression index  $\lambda^*$ . This means that  $\lambda^*$  and  $\mu^*$  depend on each other or the ratio of them is about constant (Mesri and Godlewski 1977; Mesri and Castro 1987). Both parameters are unknown along the shear zones of landslide source area S3. They were identified by varying them within large search intervals

450  
451  
452  
453  
454  
455  
456  
457  
458  
459  
460  
461  
462

**Table 6** Search intervals and fixed parameters used for the statistical analysis and the optimisation procedure (in grey, the eight parameters to be identified)

t6.1

material	parameter	unit	fixed value	vary between				constraint
				min.	max.	ln (min.)	ln (max.)	
<b>C basal shear-zone</b>	$\lambda^*$ (C)	none		0.04	1	-3.22	0	
	$\kappa^*$ (C)	none	0.02					
	$\mu^*$ (C)	none		0.00				
	$\mu^*$ (C)	none		1	0.5	-6.91	-0.69	$\mu^* (C) < 0.5 \lambda^* (C)$
	$\varphi$ (C)	°		15	25			
$c$ (C)	kN/m <sup>2</sup>		0.3					
<b>D1 secondary shear-zone of front block</b>	$\lambda^*$ (D1)	none		$\lambda^* (D1) = \lambda^* (C)$				
	$\kappa^*$ (D1)	none	0.02					
	$\mu^*$ (D1)	none		$\mu^* (D1) = \mu^* (D2)$				
	$\varphi$ (D1)	°		15	25			
	$c$ (D1)	kN/m <sup>2</sup>		0.3				
<b>D2 secondary shear-zones of active shallow landslides</b>	$\lambda^*$ (D2)	none		0.04	1	-3.22	0	$\lambda^* (D2) > \lambda^* (C)$
	$\kappa^*$ (D2)	none	0.02					
	$\mu^*$ (D2)	none		0.00				
	$\mu^*$ (D2)	none		1	0.5	-6.91	-0.69	$\mu^* (D2) < 0.5 \mu^* (C)$
	$\varphi$ (D2)	°		15	25			
$c$ (D2)	kN/m <sup>2</sup>		0.3					
<b>D3 secondary shear-zone (uppermost part)</b>	$\lambda^*$ (D3)	none		$\lambda^* (D3) = \lambda^* (D2)$				
	$\kappa^*$ (D3)	none	0.02					
	$\mu^*$ (D3)	none		$\mu^* (D3) = \mu^* (D2)$				
	$\varphi$ (D3)	°		$\varphi (D3) = \varphi (D2)$				
	$c$ (D3)	kN/m <sup>2</sup>			5	50		

In spite of linking a number of parameters, still, eight parameters remain to be identified, namely  $\lambda^*$  (C),  $\mu^*$  (C),  $\varphi$  (C),  $\varphi$  (D1),  $\lambda^*$  (D2),  $\mu^*$  (D2),  $\varphi$  (D2) and  $c$  (D3). A statistical analysis, based on 7,670 calls of the forward calculation, was carried out on these eight parameters, varying them within the intervals specified in Table 6. The corresponding scatter-plot matrix is presented in Fig. 8

463 (Table 6). As a result of the long-term displacements (up to 75 cm  
 464 in 2001–2004 monitoring period), residual strength conditions  
 465 were assumed. Accordingly, an arbitrary value of 0.3 kN/m<sup>2</sup> has  
 466 been used for residual cohesion in order to avoid numerical  
 467 instability in the calculations. Due to the situation that in shear-  
 468 zone domain D3, the activity rate is lower (cumulative displacements  
 469 from 5 to 30 cm in 2001–2004 monitoring period) and it was  
 470 assumed that the corresponding shear surface is not fully devel-  
 471 oped and strength is not fully softened. Therefore, a search inter-  
 472 val for cohesion also was adopted here (Table 6). Representative  
 473 values of the friction angle  $\phi$  are assumed to be controlled also by  
 474 the presence of coarser components, such as rock blocks. Conse-  
 475 quently, the friction angles of the shear zones were selected to be  
 476 identified, varying them between 15° and 25°, i.e. the estimated

residual friction angle of the soil matrix and the friction angle of  
 bedrock in heavily weathered condition (Panizza et al. 2006). The  
 modified swelling index of  $\kappa^*$  was fixed based on laboratory data:  
 Values obtained in five oedometer tests on different samples from  
 the soil matrix of the landslide material (fraction <2 mm) ranged  
 between 0.01 and 0.05, with an average value of 0.026. Due to the  
 influence of less deformable coarser components, representative  
 values of  $\kappa^*$  for the shear zones were assumed to be lower, i.e.  
 stiffness is higher than that of the fine-grained fraction. Therefore,  
 the value of 0.02 was used. To avoid physically and numerically  
 unfavourable parameter combinations and to minimise the number  
 of unsuccessful attempts, two parameter constraints were  
 prescribed in all parameter sets, based on literature and lab data:  
 The highest  $\mu^*$  value be smaller than half of the lowest  $\lambda^*$  value. A

477  
 478  
 479  
 480  
 481  
 482  
 483  
 484  
 485  
 486  
 487  
 488  
 489  
 490

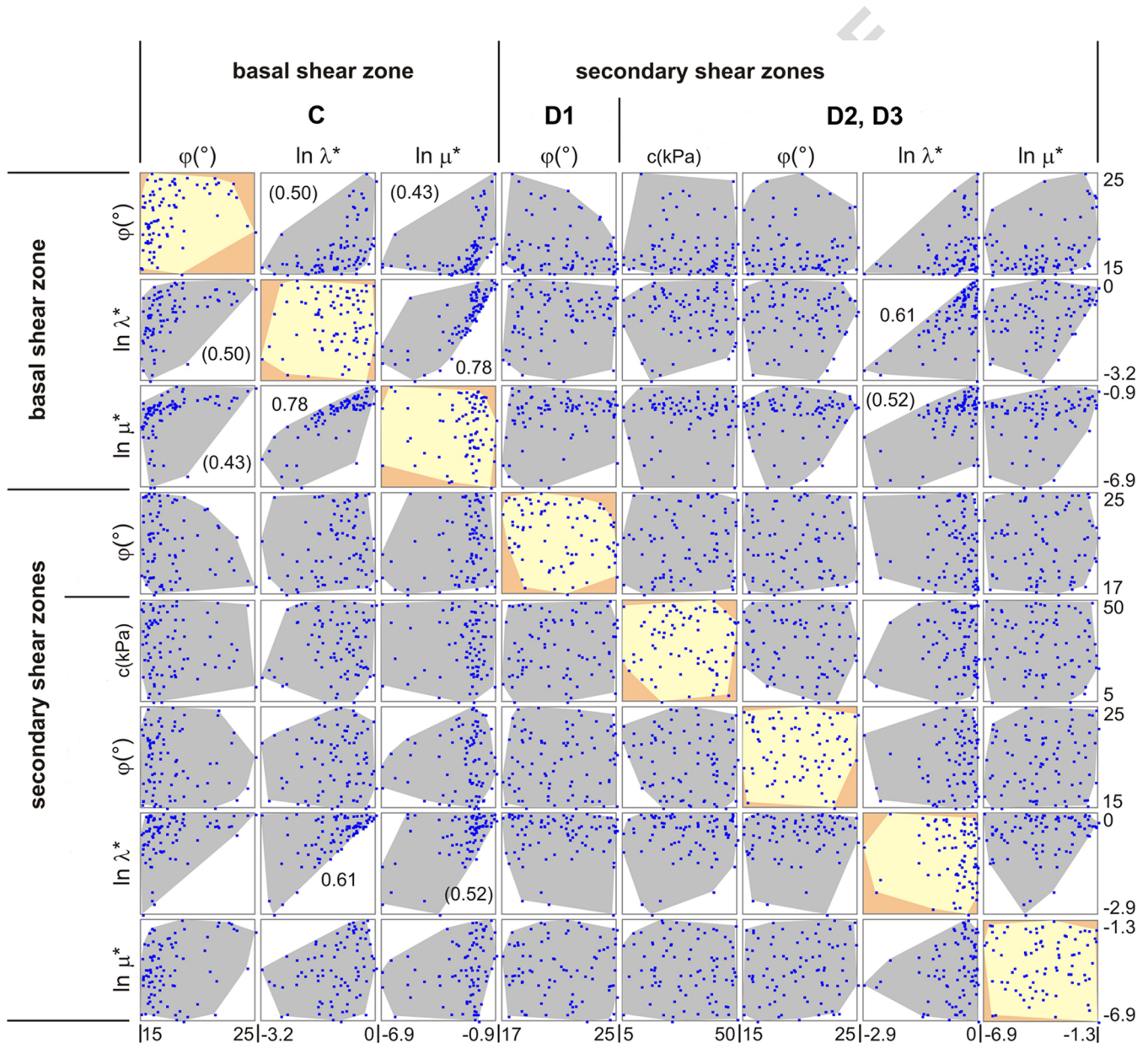


**Fig. 8** Scatter-plot matrix for the slope model. Basal shear zone C and Secondary shear zones D1, D2 and D3 (see Fig. 5 and Table 6). The numbers are 2D linear correlation coefficients as described in Section 3 and Fig. 6. In case the coefficient falls below 0.6, the numbers are in brackets. In case the coefficient is below 0.3 no number is shown

491 summary of all above-described parameter links and parameter  
492 constraints is given in Table 6.

493 To indicate the expected shape and location of the optimal  
494 value range, this matrix shows only the parameter combina-  
495 tions related to the 83 lowest objective function values (marked  
496 by blue points in the matrix). None of the plots of the scatter-  
497 plot matrix have a clear-cut shape; therefore, the problem must  
498 be considered as underdetermined and it is advisable not to  
499 increase the number of varying parameters. However, the ob-  
500 jective function plots give some pieces of information as to the  
501 most probable ranges of the best parameter values. For the  
502 friction angle  $\varphi$  of the basal shear zone C, the best parameter  
503 sets are all located in the lower part of the search interval, i.e.  
504 between  $15^\circ$  and  $19^\circ$ , whereas for  $\mu^*$  of this zone, they accu-  
505 mulate in the upper part of the interval. Less clearly, this can  
506 be noticed also for the values of  $\lambda^*$ , because  $\mu^*$  and  $\lambda^*$  appear  
507 to be correlated (linear correlation coefficient of 0.78), as  
508 previously expected. None of the 83 best parameter combina-  
509 tions have a value of  $\mu^*$  in the uppermost part of the search  
510 interval, i.e. between logarithmised  $\mu^*$  values of  $-0.9$  and  
511  $-0.69$ . The information obtained for the parameters of the  
512 secondary shear zones D1, D2 and D3 is less clear. As in none  
513 of the displayed best parameter sets  $\varphi$  of the front slide (D1) is  
514 below  $17^\circ$  and furthermore in 15 of the 18 best sets,  $\varphi$  values  
515 are between  $18^\circ$  and  $23^\circ$ , and the statistical analysis indicates  
516 that an optimum value of this parameter can be identified in  
517 the medium range of the search interval. Relatively good  
518 objective function values can be obtained independent of the  
519 cohesion value assigned to shear-zone domain D3, except for  
520 values from the lowermost part of the interval. In contrast,  
521 relatively good fits are observed for a wide range of friction  
522 angles of D3 but not for values from the uppermost part of  
523 the search interval. In the case of  $\lambda^*$  for shallow landslides, the  
524 accumulation of plotted points on the right side of the interval  
525 as well as the weak correlation between  $\lambda^*(C)$  and  $\lambda^*(D2, D3)$   
526 are direct consequences of the parameter constraint demand-  
527 ing for  $\lambda^*(D2, D3) > \lambda^*(C)$ . The objective function projection  
528 for the parameter  $\mu^*$  of these layers shows good model fits  
529 independent of the parameter value, except for the uppermost  
530 part of the search interval (between logarithmised  $\mu^*$  values of  
531  $-1.3$  and  $-0.69$ ) where none of the 83 best parameter sets are  
532 plotted. From the scatter-plot matrix in Fig. 8, it is not clear  
533 whether the search interval for  $\lambda^*$  of the shear zones of the  
534 shallow landslides (D2 and D3) is sufficient since the data  
535 points with low deviation values accumulate near the upper  
536 boundary. As for higher values of  $\lambda^*$  (e.g. between 1 and 2,  
537 logarithmised values between 0 and 0.69), the percentage of  
538 failed forward calculations increased considerably and it was  
539 decided not to enlarge the interval.

540 **Identification of shear-zone parameters with the SCE algorithm**

541 After the statistical analysis, the search intervals presented in Table 6  
542 were used also for the optimisation procedure applying the SCE  
543 algorithm, as described in the “Inverse parameter identification  
544 technique” section. After 1,100 calls of the forward calculation, the  
545 SCE algorithm was not able to further reduce the objective function  
546 value. The lowest value reached  $9.2 \times 10^{-4}$ . The parameter sets iden-  
547 tified by the algorithm using the complete reference dataset are  
548 shown in Table 7.

Table 7 Relative errors between simulated horizontal displacements and GPS measurements at points 23–28 [(measured – calculated) / measured] in the two steps of the calibration procedure (1: first step optimisation; 2: second step optimisation)

GPS point	Step	GPS Survey											
		Sep 01	Jun 02	Aug 02	Sep 02	Oct 02	Jun 03	Aug 03	Sep 03	Jun 04	Aug 04	Oct 04	
23	1	0	-0.11	-0.12	-0.13	-0.15	-0.01	-0.01	-0.02	0.11	0.15	0.11	0.11
	2	0	-0.18	-0.18	-0.19	-0.20	-0.11	-0.11	-0.11	0.02	0.07	0.01	0.01
24	1	0	-0.72	-0.28	-0.32	-0.31	-0.07	-0.21	-0.18	0.02	0.04	0.03	0.03
	2	0	-0.78	-0.37	-0.40	-0.39	-0.10	-0.27	-0.24	-0.01	0.00	0.00	0.00
25	1	0	-0.38	-0.34	-0.35	-0.45	-0.04	-0.09	-0.08	0.07	0.05	0.04	0.04
	2	0	-0.52	-0.45	-0.45	-0.57	-0.13	-0.18	-0.17	0.00	-0.03	-0.04	-0.04
26	1	0	-0.50	-0.43	-0.27	-0.30	-0.05	-0.17	-0.09	0.10	0.08	0.10	0.10
	2	0	-0.56	-0.54	-0.36	-0.40	-0.09	-0.24	-0.16	0.06	0.03	0.06	0.06
27	1	0	-2.54	-0.80	-0.79	-0.88	-0.27	-0.30	-0.39	-0.13	-0.14	-0.10	-0.10
	2	0	-2.97	-0.98	-0.95	-1.04	-0.40	-0.41	-0.50	-0.22	-0.23	-0.20	-0.20
28	1	0	-1.11	-0.74	-0.84	-0.82	-0.04	-0.03	-0.06	0.11	0.22	0.21	0.21
	2	0	-1.44	-0.97	-1.08	-1.06	-0.19	-0.17	-0.20	-0.02	0.10	0.09	0.09

In the second step optimisation, a narrowed dataset was used (GPS benchmarks 23, 25 and 28)

549 In Fig. 9, the results of a calculation using the best parameter  
 550 set of the first step of the optimisation procedure can be compared  
 551 to the measured horizontal displacements of GPS points 23 to 28.  
 552 Considering the simplifications made in the model, it can be stated  
 553 that displacements are reproduced quite well for most points, but  
 554 underestimation occurs at GPS points 23 and 28. As these points lie  
 555 above secondary shear zones, in a second step of the optimisation  
 556 procedure, the parameters of the basal shear zone were fixed  
 557 at the identified best values. In this phase, a narrowed dataset  
 558 was used, containing only horizontal displacements of the  
 559 three measurement points located above secondary shear

zones (points 23, 25 and 28). A total of six parameters were 560  
 varied in the second step of the optimisation procedure. For 561  
 the search, the configuration of parameter links, parameter 562  
 constraints and search intervals was in fact modified in some 563  
 details: The optimisation algorithm was allowed to vary the 564  
 friction angle of D<sub>3</sub> shear-zone domain independently of that 565  
 of D<sub>2</sub>. When fixing the parameters of the basal shear zone, 566  
 the parameter constraint demanding for  $\lambda^*(C) < \lambda^*(D_2, D_3)$  567  
 was removed because it was preferred not to restrict the 568  
 search based on a value of an identified parameter set. After 569  
 2,092 calls, the optimisation was stopped because no 570

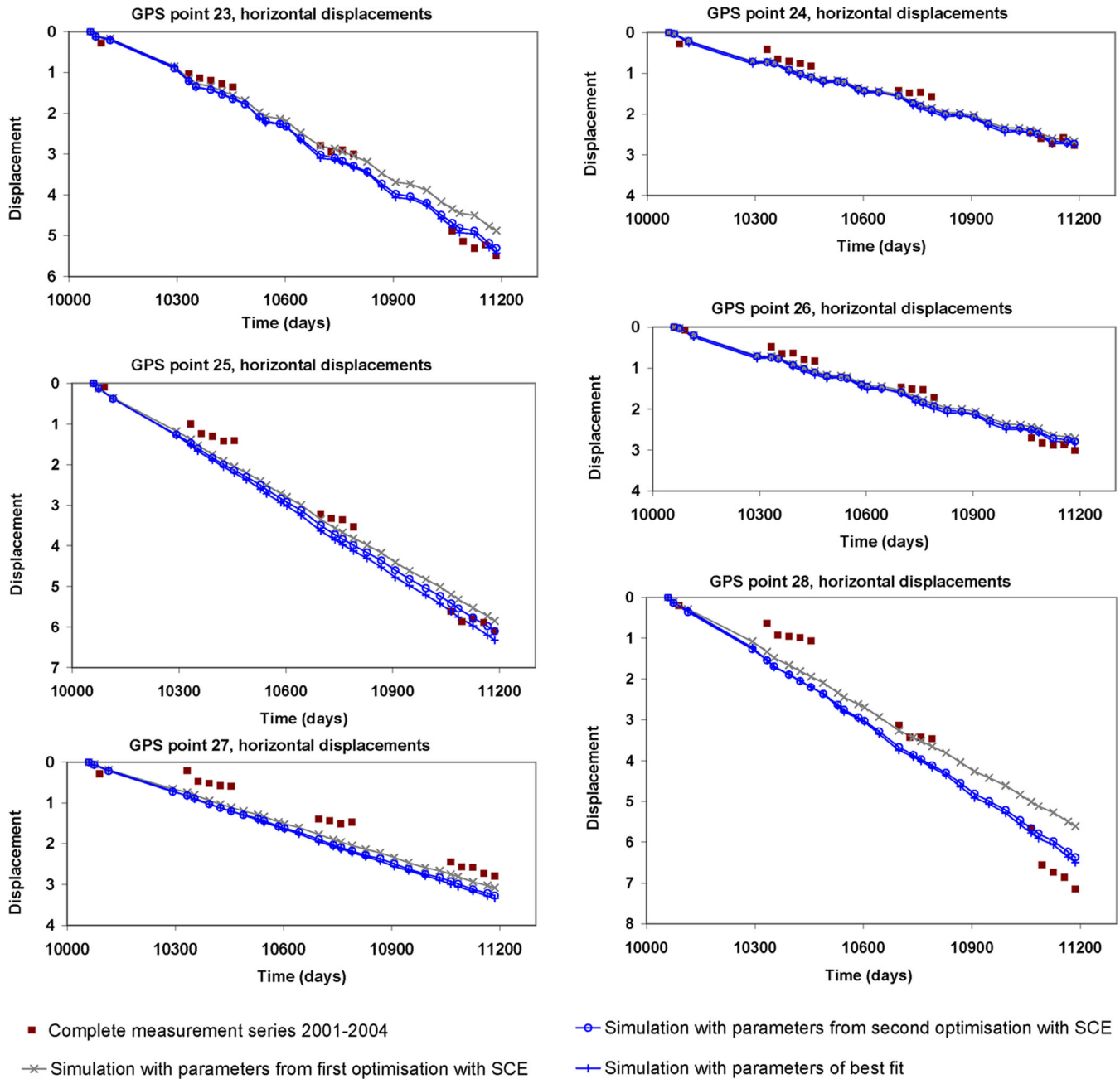


**Fig. 9** Time series of calculated displacements and measured data for GPS points 23–28 (displacements in dm)

t8.1 **Table 8** Summary of parameter values identified with SCE algorithm for the slope model

Parameter (unit)	$\lambda^*$		$\mu^*$		$\phi$ (°)				$c$ (kN/m <sup>2</sup> )	
	Zones	C, D1	D2, D3	C	D1, D2, D3	C	D1	D2		D3
Complete dataset		0.62	0.96	0.17	0.31	18.1	21.6	16.2	16.2	48.3
Narrowed dataset		Fixed	0.63	Fixed	0.24	Fixed	19.5	16.4	23.8	16.9

t8.2  
t8.3  
t8.4

571 significant reduction of the objective function value was observed. It can be noticed that the underestimation of displacements at points 23 and 28 is reduced after the second step optimisation. The relative errors between simulated and measured values are shown in Table 7, with maximum relative errors in the order of 20 % at the end of the simulated monitoring period. The identified best parameter set is given in Table 8.

579 In Fig. 9, the second-step optimisation results are compared to the measured time series of the horizontal displacements at GPS benchmarks 23–28 (2001–2004 displacements are shown at the same time-scale for all points). For GPS benchmarks 23, 24, 25 and 26, the whole curve of the time series is nearly matching the reference data points, except for small differences, which are always below 5 cm. These benchmarks are located in the slope area where most of the hydrogeological data have been collected; hence, the simplified hydrological assumptions hold true. Conversely, the calculated displacement patterns are not curved enough, or too linear, at GPS points 25, 27 and 28. There, the displacements are smaller in summer and larger during autumn and after snowmelt infiltration. Due to the simplified hydrogeological assumptions, this seasonal phenomenon is not reproduced properly by the model. In Fig. 10, the displacement vectors calculated for the 3 years of the monitoring period (2001–2004) after the second step of optimisation are compared with those measured in the field by means of GPS. Reproduction of the horizontal displacements at the end of the monitoring period is good. Except for GPS points 26 and 28, vertical displacements are clearly overestimated, even if the low precision of the vertical displacement measurements has to be taken into account. However, the direction of the simulated displacements is subparallel to the slope, as observed in the source area of the Corvara earthflow.

603 Qualitatively, the modelled displacement profile at point 24 is in accordance with that measured by the nearby inclinometer C4. 604

605 **Conclusions**

606 The case study of the Corvara earthflow is promising, as a large amount of relevant high-quality data, obtained at several locations, mainly with continuous or semi-continuous acquisition frequency, are available. In fact, geomorphological evidence and monitoring data at the local scale were exploited in support of the development, running, calibration and validation of an FE continuum model. In particular, the model calibrated via an inverse parameter identification technique was able to simulate the displacement occurred at several monitoring points in the source area S3 with average relative errors for horizontal displacements at the end of the simulated period lower than 7 %.

618 Applying the inverse analysis makes the calibration procedure much more objective and repeatable. Beyond that, these methods provide statistical information about sensitivity and interdependence of model parameters. In principle, the definition of the overall modelled problem improves with any additional value measured in the field, and calibration quality can be quantified via the objective function. Obviously, an increase of the temporal resolution of the displacement measurements and of the spatial resolution of the pore pressure measurements could improve the calculated displacements obtained in this study. The longer and the more comprehensive the time series of measurements are, the more parameters can be identified, which until now had to be fixed based on assumptions. Quantitative results—objective function values, correlations, etc.—obtained by the statistical analyses and during the optimisation allow for judging whether a refinement of the model 633

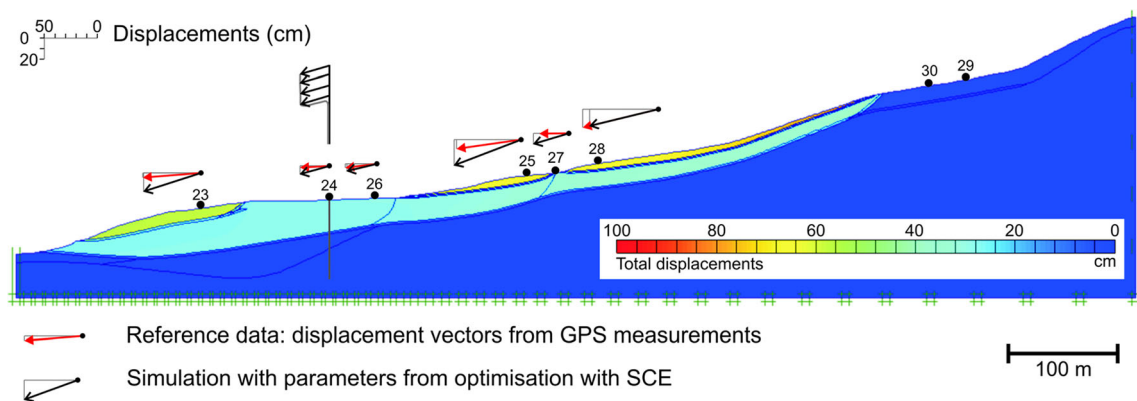


**Fig. 10** Calibrated slope model. Comparison of simulated displacement vectors with GPS field measurements during 2001–2004 period

- 634 improves its quality or if an apparently more realistic model  
 635 will lead to further uncertainty. This type of information can  
 636 hardly be gained when model calibration is performed by  
 637 means of a traditional trial-and-error procedure.
- 638  
 639 **Acknowledgments**
- 640 The German Academic Exchange Service (DAAD) and the Ateneo  
 641 Italo-Tedesco are acknowledged for funding a VIGONI 2006–2007  
 642 exchange project. DAAD granted a short research period to L.  
 643 Borgatti in 2013 which was useful to finalise the paper. Six anonym-  
 644 ous reviewers and the editor are acknowledged for their con-  
 645 structive comments.
- 646
- 647 **References**
- 648 Angeli MG, Gasparetto P, Pasuto A, Silvano S, Menotti RM (1996a) Examples of mudslides  
 649 on low-gradient clayey slopes. In: Senneset K (ed) Landslides, Proc. 7th Int. Symp.  
 650 Landslides, Trondheim. Balkema, Rotterdam 1:141–145
- 651 Angeli MG, Gasparetto P, Menotti RM, Pasuto A, Silvano S (1996b) A visco-plastic model  
 652 for slope analysis applied to a mudslide in Cortina d'Ampezzo, Italy. *Q J Eng Geol*  
 653 29:233–240
- 654 Angeli MG, Buma J, Gasparetto P, Pasuto A (1998) A combined hillslope  
 655 hydrology/stability model for low-gradient clay slopes in the Italian Dolomites.  
 656 *Eng Geol* 49:1–13
- 657 Augustesen A, Liingaard M, Lade PV (2004) Evaluation of time-dependent behaviour of  
 658 soils. *Int J Geomech* 4(3):137–156
- 659 Bonomi T, Cavallin A (1999) Three-dimensional hydrological modelling application to the  
 660 Alverà mudslide (Cortina d'Ampezzo, Italy). *Geomorphology* 30:189–199
- 661 Borgatti L, Soldati M (2010) Landslides as a geomorphological proxy for climate  
 662 change: a record from the Dolomites (Northern Italy). *Geomorphology*  
 663 120:56–64
- 664 Borgatti L, Corsini A, Marcato G, Pasuto A, Silvano S, Zabuski L (2007a) Numerical  
 665 analysis of countermeasure works influence on earth slide stabilisation: a case  
 666 study in South Tyrol (Italy). In: Proceedings of the First North American  
 667 Landslide Conference (ed) Landslides and Society: Integrated Science, Engineer-  
 668 ing Management and Mitigation. AEG, Vail (USA) 23:1007–1015
- 669 Borgatti L, Ravazzi C, Donegana M, Corsini A, Marchetti M, Soldati M (2007b) A lacustrine  
 670 record of early Holocene watershed events and vegetation history, Corvara in Badia,  
 671 Dolomites (Italy). *J Quat Sci* 22(2):173–189
- 672 Calvello M, Finno RJ (2004) Selecting parameters to optimize in model calibration by  
 673 inverse analysis. *Comput Geotech* 31:411–425
- 674 Caris JPT, van Asch T (1991) Geophysical, geotechnical and hydrological investigations of  
 675 a small landslide in the French Alps. *Eng Geol* 31(3–4):249–276
- 676 Cividini A, Jurina L, Gioda G (1981) Some aspects of characterization problems in  
 677 Geomechanics. *Int J Rock Mech Min Sci* 18(6):487–503
- 678 Comegna L, Picarelli L, Urciuoli G (2007) The mechanics of mudslides as a cyclic  
 679 undrained–drained process. *Landslides* 4(3):217–232
- 680 Corsini A (2000) L'influenza dei fenomeni franosi sull'evoluzione geomorfologica post-  
 681 glaciale dell'Alta Val Badia e della Valparola (Dolomiti). Dissertation, Università di  
 682 Bologna, Italy
- 683 Corsini A, Pasuto A, Soldati M (1999) Geomorphological investigation and man-  
 684 agement of the Corvara landslide (Dolomites, Italy). *Trans Jpn Geomorphol*  
 685 *Union* 20:169–186
- 686 Corsini A, Marchetti M, Soldati M (2001) Holoceneslope dynamics in the area of  
 687 Corvara in Badia (Dolomites, Italy). *Geografia Fisica e Dinamica Quaternaria*  
 688 24:127–139
- 689 Corsini A, Pasuto A, Soldati M, Zannoni A (2005) Field monitoring of the Corvara  
 690 landslide (Dolomites, Italy) and its relevance for hazard assessment. *Geomorphology*  
 691 66:149–165
- 692 Cruden DM, Varnes DJ (1996) Landslide types and processes. In: Turner AK, Schuster RL  
 693 (ed) Landslides: investigation and mitigation, Transportation Research Board. Special  
 694 Report 247 National Academy Press, Washington D.C
- 695 Duan QY, Sorooshian S, Gupta VK (1992) Effective and efficient global optimi-  
 696 zation for conceptual rainfall-runoff models. *Water Resour Res* 28(4):1015–  
 697 1031
- Duan QY, Gupta VK, Sorooshian S (1993) Shuffled complex evolution approach  
 for effective and efficient global minimization. *J Optim Theory Appl* 76  
 (3):501–521
- Duan QY, Sorooshian S, Gupta VK (1994) Optimal use of the SCE-UA global optimization  
 method for calibrating watershed models. *J Hydrol* 158:265–284
- Feng XT, Chen BR, Yang C, Zhou H, Ding X (2006) Identification of visco-elastic models  
 for rocks using genetic programming coupled with the modified particle swarm  
 optimization algorithm. *Int J Rock Mech Min Sci* 43:789–801
- Finsterle S (2006) Demonstration of optimization techniques for groundwater plume  
 remediation using iTOUGH2. *Environ Model Softw* 22:665–680
- Francois B, Tacher L, Bonnard C, Laloui L, Triguero V (2007) Numerical modelling of the  
 hydrogeological and geomechanical behaviour of a large slope movement: the  
 Triesenberg landslide (Liechtenstein). *Can Geotech J* 44(7):840–857
- Gens A, Ledesma A, Alonso EE (1996) Estimation of parameters in geotechnical  
 backanalysis—II. Application to a tunnel excavation problem. *Comput Geotech*  
 18:29–46
- Guzzetti F, Cardinali M, Reichenbach P (1994) The AVI project: a bibliographical  
 and archive inventory of landslides and floods in Italy. *Environ Manag* 18  
 (4):623–633
- Hvorslev M (1949) Subsurface exploration and sampling of soils for civil engineering  
 purposes. Report on soil sampling, U.S. waterways experiment station, Vicksburg, pp  
 521
- Krahn J (2004) Seepage modeling with SEEP/W. GEO-SLOPE International Ltd
- Ledesma A, Gens A, Alonso EE (1996a) Estimation of parameters in geotechnical  
 backanalysis—I. Maximum likelihood approach. *Comput Geotech* 18(1):1–27
- Ledesma A, Gens A, Alonso EE (1996b) Parameter and variance estimation in geotech-  
 nical backanalysis using prior information. *Int J Numer Anal Methods Geomech*  
 20:119–141
- Levasseur S, Malecot Y, Boulon M, Flavigny E (2008) Soil parameter identification using a  
 genetic algorithm. *Int J Numer Anal Methods Geomech* 32:189–213
- Malecot Y, Flavigny E, Boulon M (2004) Inverse analysis of soil parameters for finite  
 element simulation of geotechnical structures: pressuremeter test and excavation  
 problem. In: Brinkgreve RBJ, Schad H, Schweiger HF, Willand E (eds) Proc. Symp.  
 Geotechnical Innovations. Verlag Glückauf, Essen, pp 659–675
- Malet JP, Laigle D, Remaitre A, Maquaire O (2005) Triggering conditions and  
 mobility of debris flows associated to complex earthflows. *Geomorphology* 66  
 (1–4):215–235
- Manly BFJ (1944) Multivariate statistical methods: a primer. 3rd Edition. Chapman & Hall,  
 CRC
- Marcato G, Mantovani M, Pasuto A, Tagliavini F, Silvano S, Zabuski L (2009) Assessing the  
 possible future development of the Tessina landslide using numerical modelling. In:  
 Malet JP, Remaitre A, Bogaard T (eds) Landslide processes: from geomorphological  
 mapping to dynamic modelling. CERG, Strasbourg, France, pp 327–334
- Marcato G, Mantovani M, Pasuto A, Zabuski L, Borgatti L (2012) Monitoring, numerical  
 modelling and hazard mitigation of the Moscardo landslide (Eastern Italian Alps). *Eng*  
*Geol* 128:95–107
- Meier J (2008) Parameterbestimmung mittels inverser Verfahren für geotechnische  
 Problemstellungen. Dissertation. Bauhaus-Universität Weimar, Germany
- Meier J, Rudolph S, Schanz T (2006) Effektiver Algorithmus zur Lösung von inversen  
 Aufgabenstellungen. *Bautechnik* 83(7):470–481
- Meier J, Schädler W, Borgatti L, Corsini A, Schanz T (2008) Inverse parameter identi-  
 fication technique using PSO algorithm applied to geotechnical modeling. *Journal of*  
*Artificial Evolution and Applications*, Article ID 574613, 14 pages, doi:10.1155/2008/  
 574613
- Mesri G, Castro A (1987)  $C_u/C_c$  concept and  $K_0$  during secondary compression. *J Geotech*  
*Eng* 112(3):230–247
- Mesri G, Godlewski P (1977) Time- and stress-compressibility interrelationship. *J Geotech*  
*Eng Div* 103:417–430
- Panizza M, Silvano S, Corsini A, Soldati M, Marchetti M, Borgatti L, Ghinoi A, Piacentini D,  
 Pasuto A, Zannoni A, Marcato G, Mantovani M, Tagliavini F, Moretto S (2006)  
 Definizione della pericolosità e di possibili interventi di mitigazione della frana di  
 Corvara in Badia. Provincia Autonoma di Bolzano, Südtirol. [http://www.provinz.bz.it/  
 wasserschutzbauten/download/Download\\_Corvara\\_RelazioneFinale\\_10-4-  
 06\\_inviato.pdf](http://www.provinz.bz.it/wasserschutzbauten/download/Download_Corvara_RelazioneFinale_10-4-06_inviato.pdf) (Accessed 18 Apr 2014)
- Picarelli L, Russo C, Urciuoli G (1995) Modelling earthflow movement based on experi-  
 ences. In: Danish Geotechnical Society (ed) Proceedings of the 11th European  
 conference on soil mechanics and foundation engineering, Copenhagen, 6:157–162
- Picarelli L, Di Maio C, Olivares L, Urciuoli G (2000) Properties and behaviour of tectonized  
 clay shales in Italy. Keynote lecture, Proc. II Int. Symposium on Hard Soils and Soft  
 Rocks, Napoli, Italy 1998, Balkema, Rotterdam, 1211–1242

768	PLAXIS V8 (2003) Reference manual. In: Brinkgreve RBJ (in cooperation with: Al-Khoury R, Bakker KJ, Bonnier PG, Brand PJW, Broere W, Burd HJ, Soltys G, Vermeer PA, Vogt-Breier C, Waterman D, Den Haag DOC. Technical University of Delft and PLAXIS BV, The Netherlands	Vulliet L, Bonnard C (1996) The Chlówena landslide: prediction with a viscous model. In VIIIth Int. Symp. on landslides. Trondheim 1:397–402	799
769	R, Bakker KJ, Bonnier PG, Brand PJW, Broere W, Burd HJ, Soltys G, Vermeer PA, Vogt-Breier C, Waterman D, Den Haag DOC. Technical University of Delft and PLAXIS BV, The Netherlands	Zhang ZF, Ward AL, Gee GW (2003) Estimating soil hydraulic parameters of a field drainage experiment using inverse techniques. Vadose Zone J 2:201–211	800
770	Schädler W (2008) Slope movements of the earthflow type—engineering-geological investigation, geotechnical assessment and modelling of the source areas on the basis of case studies from the Alps and Apennines. Dissertation at Friedrich-Alexander-Universität Erlangen-Nürnberg. Logos Verlag Berlin GmbH, pp 212		801
771	Schanz T, Meier J (2008) Gestaltung, Validierung und Optimierung von Messprogrammen für geotechnische Aufgabenstellungen. Bautechnik 85(5):307–316		802
772	Schanz T, Zimmerer MM, Datcheva M, Meier J (2006) Identification of constitutive parameters for numerical models via inverse approach. Felsbaumagazin 24 (2):11–21		803
773	Schwarz S (2001) Sensitivitätsanalyse und Optimierung bei nicht linearen Strukturverhalten. Institute für Baustatik, Universität Stuttgart, Bericht 34		804
774	Soldati M, Corsini A, Pasuto A (2004) Landslides and climate change in the Italian Dolomites since the Late Glacial. Catena 55:141–161		805
775	Tacher L, Bonnard C, Laloui L, Parriaux A (2005) Modelling the behaviour of a large landslide with respect to hydrogeological and geomechanical parameter heterogeneity. Landslides 2(1):3–14		806
776	Thornthwaite CW (1948) An approach toward a rational classification of climate. Geogr Rev 38:55–94		807
777	Trigila A, Iadanza C, Spizzichino D (2010) Quality assessment of the Italian Landslide Inventory using GIS processing. Landslides 7(4):455–470		808
778	van Asch T, van Beek LPH, Bogaard TA (2007) Problems in predicting the mobility of slow-moving landslides. Eng Geol 91:46–55		809
779	Vermeer PA, Neher HP (1999) A soft soil model that accounts for creep. In: Proceedings of the International Symposium (ed) Beyond 2000 in Computational Geotechnics—10 Years of PLAXIS International. Balkema, Amsterdam, pp 249–261		810
780			811
781			812
782			813
783			814
784			815
785			816
786			817
787			818
788			819
789			820
790			821
791			822
792			823
793			824
794			825
795			806Q1

### W. Schädler

WPW Geoconsult Südwest GmbH,  
Erzbergerstraße 19, 68165 Mannheim, Germany

### L. Borgatti

Department of Civil, Chemical, Environmental and Materials Engineering DICAM, ALMA MATER STUDIO RUM,  
University of Bologna,  
Viale Risorgimento 2, 40136 Bologna, Italy  
e-mail: lisa.borgatti@unibo.it

### A. Corsini · F. Ronchetti

Department of Chemical and Geological Sciences DSCG,  
University of Modena and Reggio Emilia,  
Largo Sant'Eufemia 19, 41121 Modena, Italy

### J. Meier

Gruner AG,  
Gellertstrasse 55, 4020 Basel, Switzerland

### T. Schanz

Foundation Engineering, Soil and Rock Mechanics, Faculty of Civil and Environmental Engineering,  
Ruhr-Universität Bochum,  
Building IC 5, Universitätsstrasse 150, 44780 Bochum, Germany

UNCORRECTED PROOF

## AUTHOR QUERIES

**AUTHOR PLEASE ANSWER ALL QUERIES.**



- Q1. Please check if affiliations are presented correctly.
- Q2. Please indicate the significance of the asterisk in Table 5.
- Q3. Please check Tables 1-8 if captured and presented correctly.

UNCORRECTED PROOF